# Mapping Impact of Urbanization in the Continental U.S. from 2001-2020

Lahouari Bounoua, Biospheric Sciences, NASA GSFC, Joseph Nigro, Biospheric Sciences, NASA GSFC and SSAI, Ping Zhang, Biospheric Sciences, NASA GSFC and University of Maryland Kurtis Thome, Biospheric Sciences, NASA GSFC

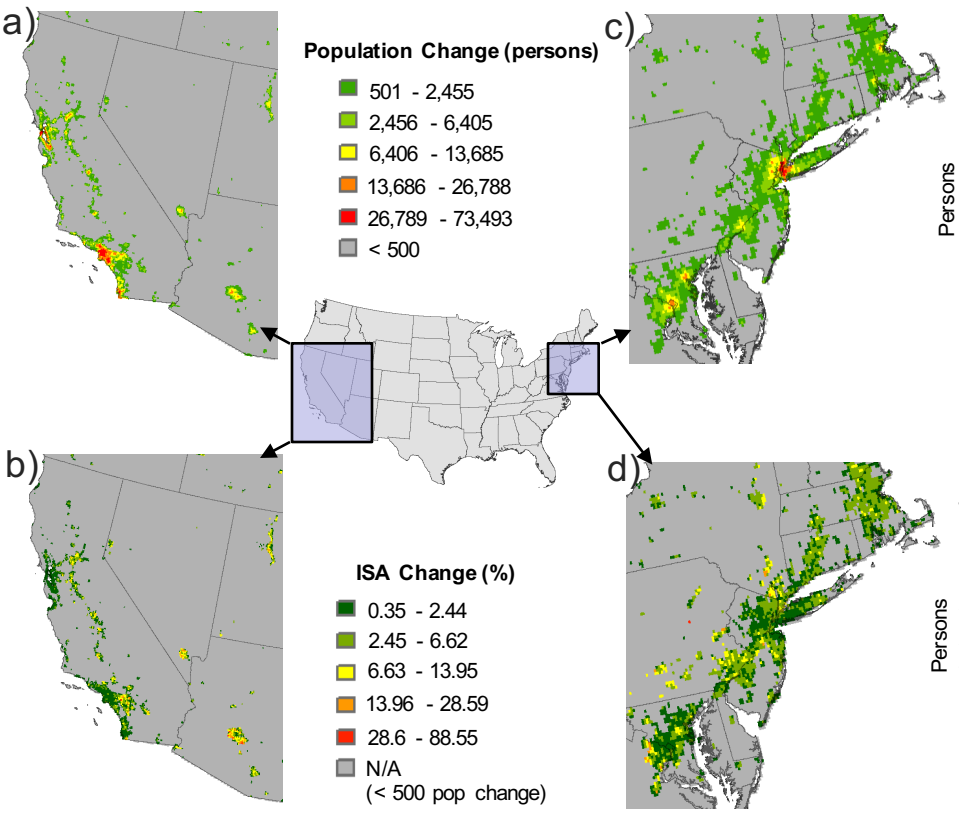


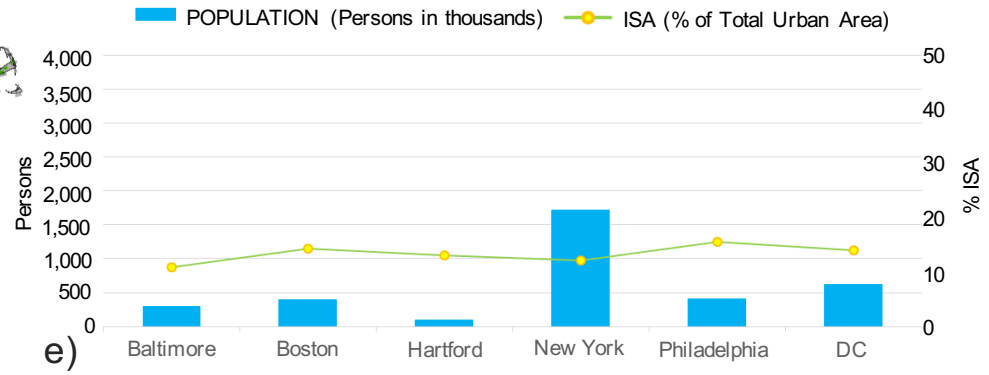


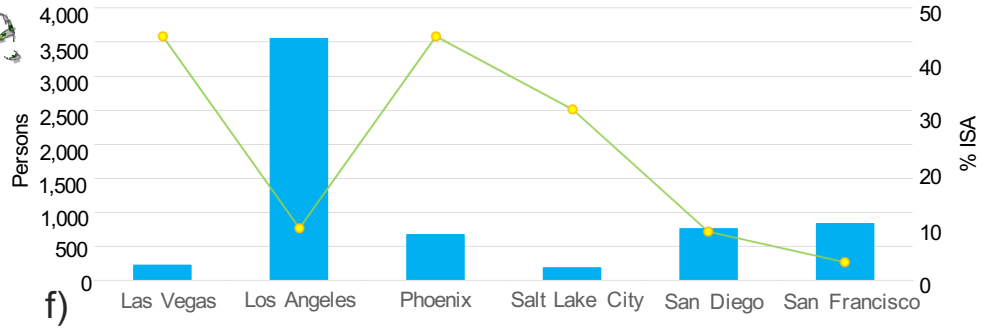


Data fusion, from Landsat and MODIS, was used to characterize US buildup and to derive a plausible 2020 impervious surface area (ISA) projection based on observed rates of ISA change as a function of population from 2006 to 2011. The analysis shows that urbanization in the U.S. implicitly includes a 'cultural character' whereby depending on the region, cities are either built horizontally with large ISA per capita or vertically with a minimal spatial footprint. This 'cultural character' can also be forced by land availability, topography and inland water. In other regions, cities seem to have adapted to their population growth and adjusted their ISA use per capita.

Name: Lahouari Bounoua, Biospheric Sciences, NASA GSFC
E-mail: Lahouari.Bounoua@nasa.gov
Phone: 301-614-6631

**References:**

Bounoua L., Nigro J., P. Zhang, K. Thome: Mapping Impact of Urbanization in the Continental U.S. from 2001-2020, in preparation.

**Data Sources:** Landsat-based National Land Cover Dataset to characterize the impervious surface area (urban) and MODIS 500m-land cover classification along with the CIESIN Gridded Population of the World and the U.S. Census Bureau 2020 National Population Projection. The 1:500k USA Urban Area boundaries (Esri, Department of Commerce, Census Bureau, Geography Division) were used to calculate population and ISA statistics within each urban area.

**Technical Description of Figures:**

***Maps:*** **a)** 2001-2020 population change in persons for the southwestern region of the U.S; **b)** 2001-2020 ISA change (% of urban area as demarcated by the 1:500k USA Urban Area boundaries) for the southwestern region of the U.S. The major urban areas included in a) and b) are Las Vegas, Los Angeles, Phoenix, Salt Lake City, San Diego, and San Francisco; **c)** 2001-2020 population change in persons for the northeastern region of the U.S; **d)** 2001-2020 ISA change (% of urban area as demarcated by the 1:500k USA Urban Area boundaries) for the northeastern region of the U.S. The major urban areas included in c) and d) are Baltimore, Boston, Hartford, New York City, Philadelphia, and Washington D.C. The table below lists 2001-2020 population and ISA change for these select urban areas.

| Urban Area | Population (persons) | ISA (%) | Urban Area | Population (persons) | ISA (%) |
|---|---|---|---|---|---|
| Baltimore, MD | 291,110 | 10.94 | Las Vegas-Henderson, NV | 230,182 | 44.76 |
| Boston, MA--NH--RI | 391,812 | 14.29 | Los Angeles-Long Beach-Anaheim, CA | 3,552,181 | 9.55 |
| Hartford, CT | 90,467 | 13.16 | Phoenix-Mesa, AZ | 669,737 | 44.76 |
| New York-Newark, NY-NJ-CT | 1,712,144 | 12.14 | Salt Lake City-West Valley City, UT | 189,288 | 31.38 |
| Philadelphia, PA--NJ--DE--MD | 405,285 | 15.55 | San Diego, CA | 762,902 | 9.01 |
| Washington, DC--VA--MD | 622,948 | 14.05 | San Francisco-Oakland, CA | 839,030 | 3.40 |

***Graphs: e)*** 2001-2020 population change vs. ISA change for select urban areas in the northeastern region of the U.S. Note that for New York City there is a projected increase in population of ~2 million people while for Hartford the population increase is only ~90,000 people, yet the ISA change for both cities is about the same. This reflects the vertical growth that is occurring in the New York City area where population use of per capita ISA is minimal compared to Hartford . ***f)*** 2001-2020 population change vs. ISA change for select urban areas in the southwestern region of the U.S. Note that for Los Angeles ISA change is small despite the projected increase in population of ~3.5 million people. In contrast, for Phoenix a smaller change in population triggers a greater increase in ISA. These examples reveal the horizontal vs. vertical building patterns and do represent regional 'cultures'.

**Scientific significance, societal relevance, and relationships to future missions:**

*Scientific significance:* 1) Urbanization in the U.S. includes a 'cultural character' whereby depending on the region, cities are either built horizontally resulting a large spatial footprint or vertically with a minimal spatial footprint despite the magnitude in population increase. 2) In some regions, cities seem to have adapted to their population growth and adjusted their ISA use per capita.

*Societal relevance:* US cities are home to more than 50% of the population and this is where climate change will be felt the most.

*Relationships to future missions:* Defines the need for a high resolution global mapping of urban settings to assess their interaction with the global environment.

# Progress of Improving Terra MODIS LWIR Spectral Band Calibration

Jack Xiong, Biospheric Sciences, NASA GSFC, Truman Wilson, Biospheric Sciences, NASA GSFC and SSAI, and Junqiang Sun, Biospheric Sciences, NASA GSFC and GST

(a)

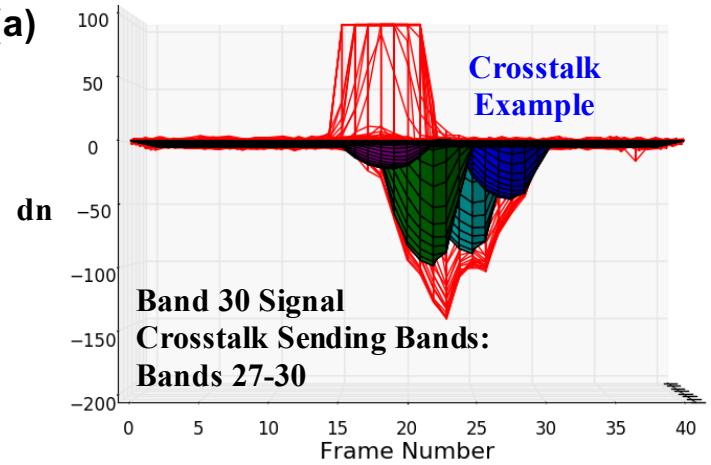


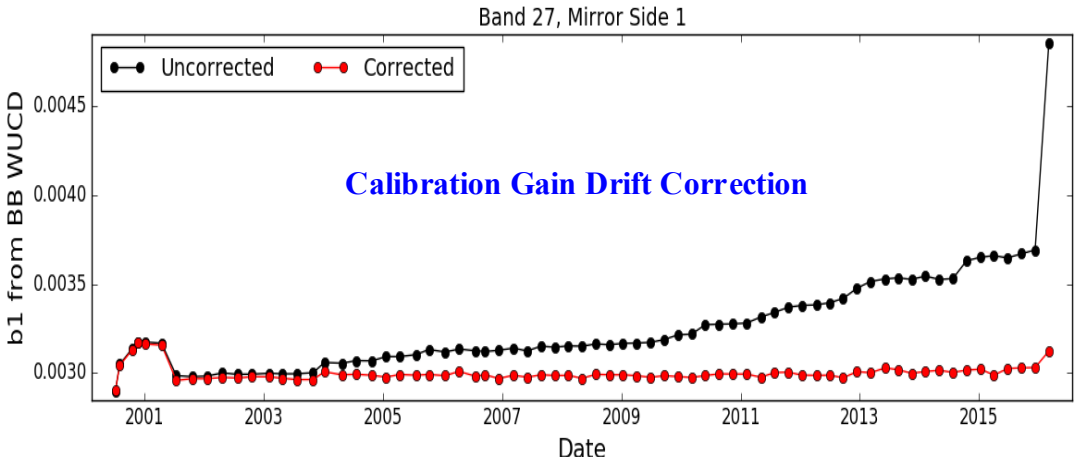


(b)

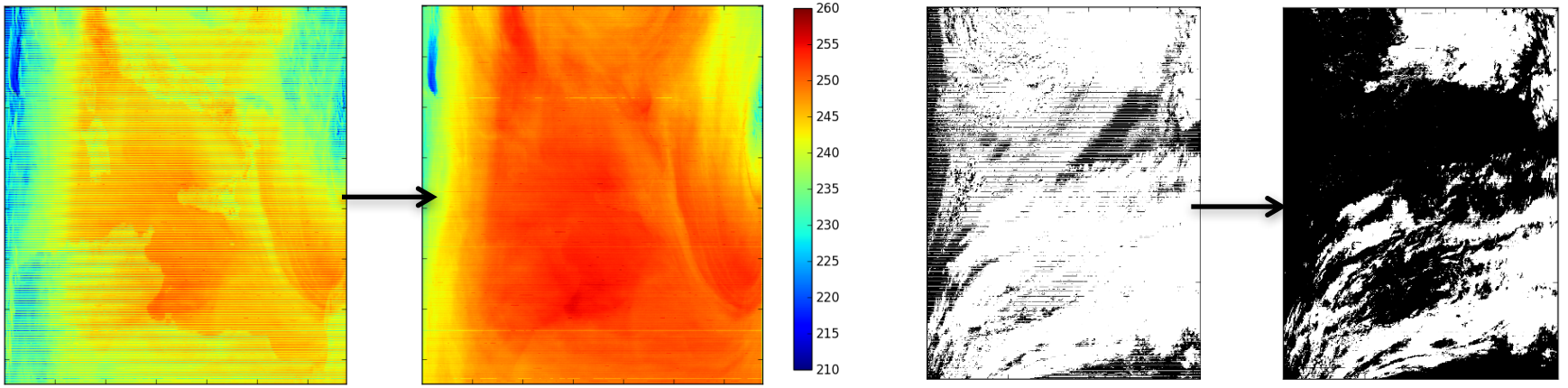


De-striping and Land Feature Removal in Band 27

Removal of False Clouds from B29 – B31 Cloud Mask

Restoring Terra MODIS LWIR spectral band calibration and data quality using improved crosstalk correction algorithm and coefficients derived from on-orbit lunar observations.

Name: Jack Xiong, NASA/GSFC, Code 618
E-mail: Xiaoxiong.Xiong-1@nasa.gov
Phone: 301-614-5957

**References:**
MCST Presentation at MODIS and VIIRS Calibration Workshop, MODIS and VIIRS Science Team Meeting June 6-10, 2016
Sun, J., X. Xiong, Y. Li, S. Madhavan, A. Wu, and B. N. Wenny, "Evaluation of Radiometric Improvements With Electronic Crosstalk Correction for Terra MODIS Band 27," IEEE Transactions on Geoscience and Remote Sensing, vol. 52, issue 10, pp. 6497 - 6507, Oct 2014
Xiong, X., Z. Wang, J. Sun, A. Angal, J. Fulbright, and J. Butler, "MODIS and VIIRS lunar observations and applications," Proc. SPIE 8889, Sensors, Systems, and Next-Generation Satellites XVII, 88890V, 2013

**Data Sources:** All sensor calibration raw data and the data used to generate the images and science product examples are from NASA GSFC Level 1 and Atmosphere Archive and Distribution System (LAADS). The calibration coefficients and crosstalk correction coefficients are derived by the NASA MODIS Characterization Support Team (MCST).

**Technical Description of Figures:**
***Graphic a):*** Terra MODIS LWIR spectral band crosstalk example for receiving band 30 and sending band from 27 to 30 (left). Illustration of band 27 calibration gain drift correction (right). The calibration gains (before and after correction) are computed using on-board blackbody observations.
***Graphic b):*** Examples of de-striping and land feature removal in Terra MODIS band 27 (data granule: 2015183.1005) and removal of false clouds from B29 – B31 Cloud Mask (data granule: 2015182.1345).

**Scientific significance, societal relevance, and relationships to future missions:** Terra MODIS has successfully operated for more than 16 years since its launch in December 1999 and its data products have been widely used by the remote sensing community and users worldwide for studies of many key environmental parameters of the earth's system. Electronic crosstalk in the LWIR PV bands (27-30) was initially identified pre-launch and its impact has become more server as mission continues to operate beyond its design lifetime. Correction algorithms have been developed and improved by previous and current MCST members to restore Terra MODIS LWIR spectral band calibration and data product quality. Implementation of crosstalk correction will be made after vigorous science and impact analyses. Approaches developed from MODIS crosstalk characterization and removal have potential applications for future remote sensing sensors, such as JPSS VIIRS and GOES-R ABI.

# Dramatic Contrasts in Arctic vs Antarctic Sea Ice Trends in 3-D Visualizations and Compilations of Monthly Record Highs and Lows

Claire L. Parkinson, Cryospheric Sciences, NASA GSFC, and Nicolo E. DiGirolamo, Cryospheric Sciences, NASA GSFC and SSAI

3-D visualizations of the month-by-month rankings of Arctic and Antarctic sea ice extents

(a) Arctic

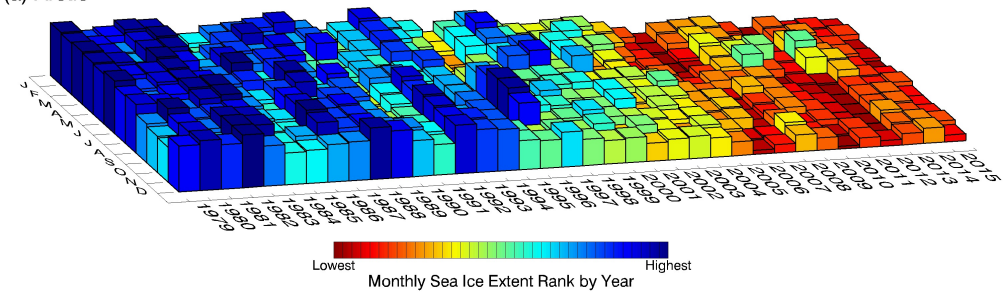


(b) Antarctic

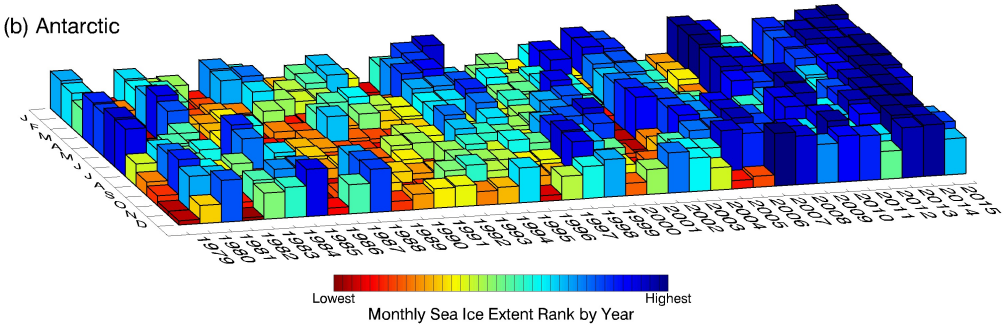


(a) Arctic record highs (●) and lows (●)

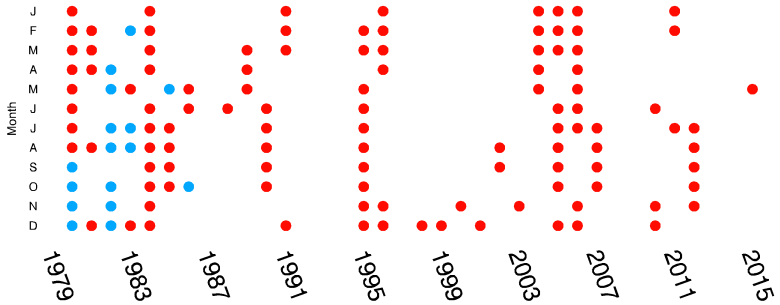


(b) Antarctic record highs (●) and lows (●)

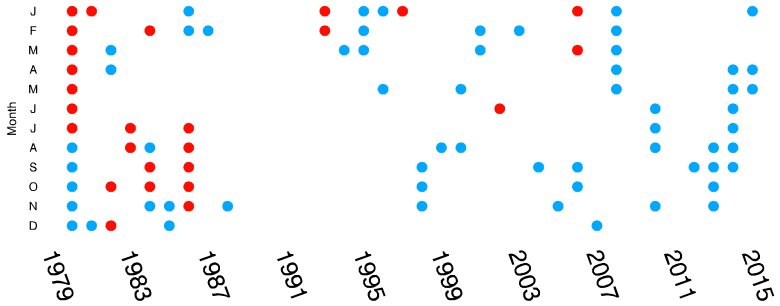


New visualizations dramatically display the decreases in Arctic sea ice coverage over the years 1979-2015, apparent in each month of the year, with not a single record high in ice extents occurring in any month since 1986, a time period with 75 monthly record lows. Results are less dramatic in the Antarctic, but intriguingly in the opposite direction, with only 6 record lows since 1986 and 45 record highs.

Names: Claire Parkinson, Cryospheric Sciences, NASA GSFC, & Nick DiGirolamo, Cryospheric Sciences, SSAI
Email: Claire.L.Parkinson@nasa.gov
Phone: 301-614-5715

**Reference:** Parkinson, C. L., and N. E. DiGirolamo, 2016: New visualizations highlight new information on the contrasting Arctic and Antarctic sea-ice trends since the late 1970s, *Remote Sensing of Environment*, 183, 198-204, doi:10.1016/j.rse.2016.05.020.

**Data Sources:** Satellite passive-microwave data from the Scanning Multichannel Microwave Radiometer (SMMR) on NASA's Nimbus 7 satellite and the Special Sensor Microwave Imager (SSMI) and SSMI Sounder (SSMIS) on satellites of the Defense Meteorological Satellite Program (DMSP).

**Technical Description of Figures:**

*Graphic 1, 3-D Visualizations*: These visualizations show for both polar regions the sea-ice-extent rankings by year for each month January–December over the 37-year period 1979-2015. For each month, the 37 years of data are ranked from rank 1 for the year with the lowest sea ice extent for that month to rank 37 for the year with the highest sea ice extent for that month; the rankings are color-coded from deep red for the lowest rank to deep blue for the highest rank. The results for the Arctic are particularly striking, with almost all the blues (high sea ice extents) in the first half of the record and almost all the reds (low sea ice extents) in the later part of the record. The Antarctic results are basically in the opposite direction, from low ranks predominantly in the early part of the record to high ranks more frequent in the later part of the record, although the upward flow for the Antarctic is not nearly as systematic as the downward flow for the Arctic.

*Graphic 2, Record Highs and Lows*: Using the satellite-derived rankings displayed in Graphic 1, the plots of Graphic 2 highlight for each month January–December every instance of a new (at the time) monthly record high ice extent (blue dots) and every instance of a new monthly record low ice extent (red dots).

**Scientific Significance:** Satellite data have revealed marked changes in Arctic and Antarctic sea ice extents since the late 1970s, contributing important information about how Earth's climate is changing. The changes in the Arctic have garnered scientific and media attention because of impacts of decreasing Arctic sea ice coverage on the Arctic climate, the Arctic ecosystems, and such individual species as the iconic polar bear. As a result, much attention has been given to each new overall record low in Arctic ice extents, these overall records typically occurring in September. This study systematically shows the record lows for all months, along with the record highs for all months, and does so for the full 37-year SMMR/SSMI/SSMIS record. The results are striking, with the loss of ice in the Arctic throughout the annual cycle so strong that there have been no monthly record high Arctic ice extents for any month of the year since 1986 but 75 monthly record lows. The Antarctic results also show a sharp contrast, although less sharp and in the opposite direction, with 6 monthly record low ice extents since 1986 and 45 monthly record highs.

# SMAP Faraday Rotation

David Le Vine, Cryospheric Sciences, NASA GSFC

Figure 1

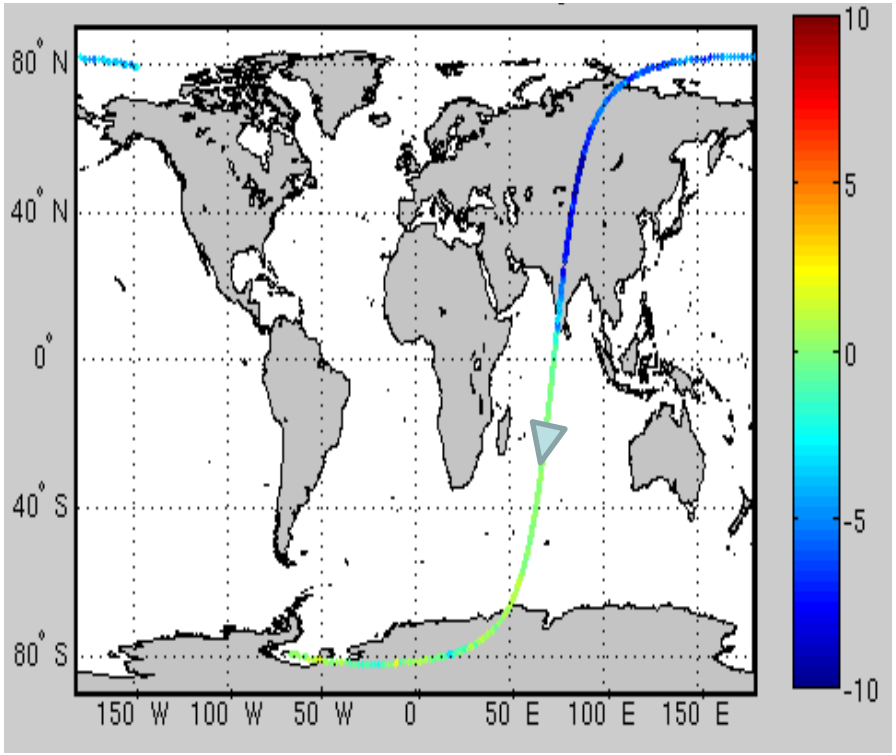


Figure 2

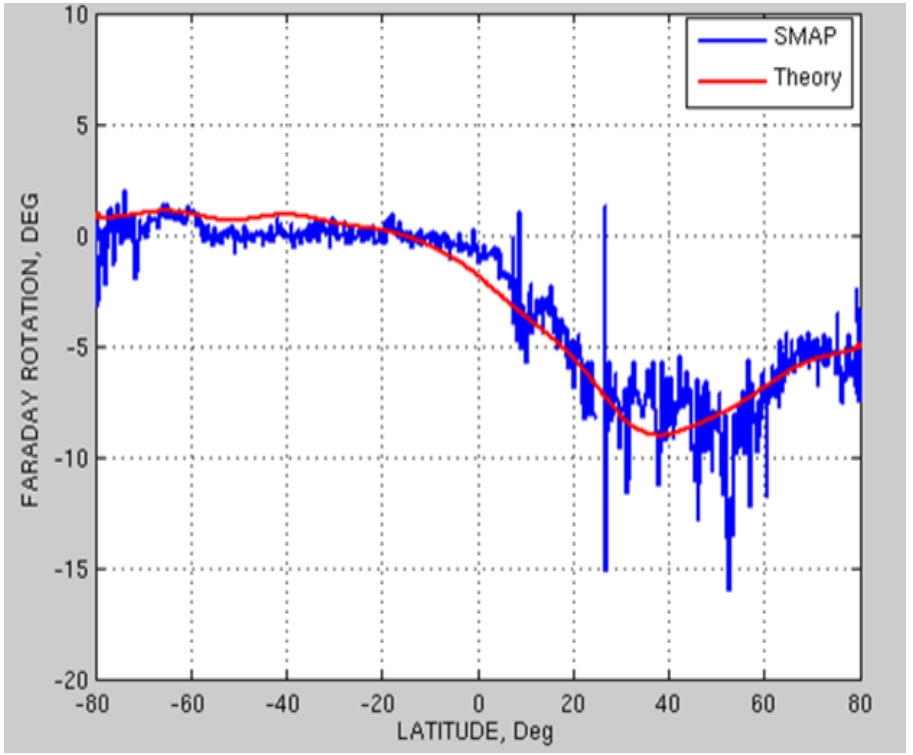


Figure 3

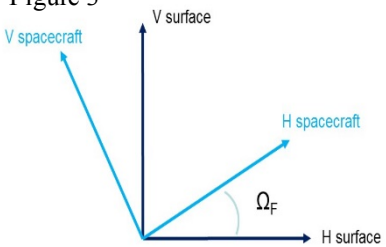


Faraday rotation is a change in the polarization as signal propagates through the ionosphere. At L-band it is necessary to correct for this change and measurements are made on the spacecraft of the rotation angle. These figures show that there is good agreement between the SMAP measurements (blue) and predictions based on models (red).

Name: David Le Vine, Cryospheric Sciences, NASA GSFC
E-mail: david.m.levine@nasa.gov
Phone: 301-614-5640

**References:**

S.H. Yueh, "Estimates of Faraday Rotation with Passive Microwave Polarimetry for Microwave Remote Sensing of Earth Surfaces", IEEE TGARS, **38** (#5), pp 2434, Sept, 2000

D.M. Le Vine et al, "Impact of Antenna Pattern on Measurement of the Third Stokes Parameter from Space at L-Band, IEEE TGARS, **49**(#1), pp 406, Jan, 2011

D. M. Le Vine et al, "Aquarius Third Stokes Parameter and Initial Resuilts", IEEE GRSL, **10** (#3), pp 520, May, 2013

D. M. Le Vine, S. Abraham and J. Peng, "Faraday Rotation Correction for the SMAP Radiometer", IEEE TGARS, 54(#4), pp 2070, April, 2016

**Data Sources:**

NASA's Soil Moisture Active Passive Mission
Aquarius Sea Surface Salinity Mission

**Technical Description of Figures:**

***Figure 1:*** Graph showing the SMAP satellite in a descending orbit.

***Figure 2:*** Graphical analysis of Faraday rotation angle retrieved from SMAP data (blue) and the theoretical prediction (red). Aquarius demonstrated the algorithm for measuring the rotation angle in situ (i.e.at the spacecraft) over the ocean for applications to the measurement of salinity [Le Vine, et al, 2013] and Aquarius data over land demonstrated some of the problems associated with the algorithm over land (e.g. noise at positive latitude) [Le Vine et al, 2011].

***Figure 3:*** The polarization rotation angle, $\Omega_F$, is measured using the ratio of the third Stokes parameter, T3, and the second Stokes parameter: Q = Tv – Th (Yueh, 2000): $\Omega_F$= - 0.5 Atan [ T3 / (Tv – Th) ]

**Scientific significance, societal relevance, and relationships to future missions:**

Faraday rotation is an important source of error in remote sensing at L-band. Research is underway to verify that the technique for measuring the rotation angle in situ using the ratio of the third and second Stokes parameter can be used by SMAP to make corrections for application to remote sensing of soil moisture [Le Vine et al, 2016].

# Rainfall-triggered Landslides Bury Sri Lankan Villages

Dalia Kirschbaum, Thomas Stanley, Hydrological Sciences, NASA GSFC, GESTAR

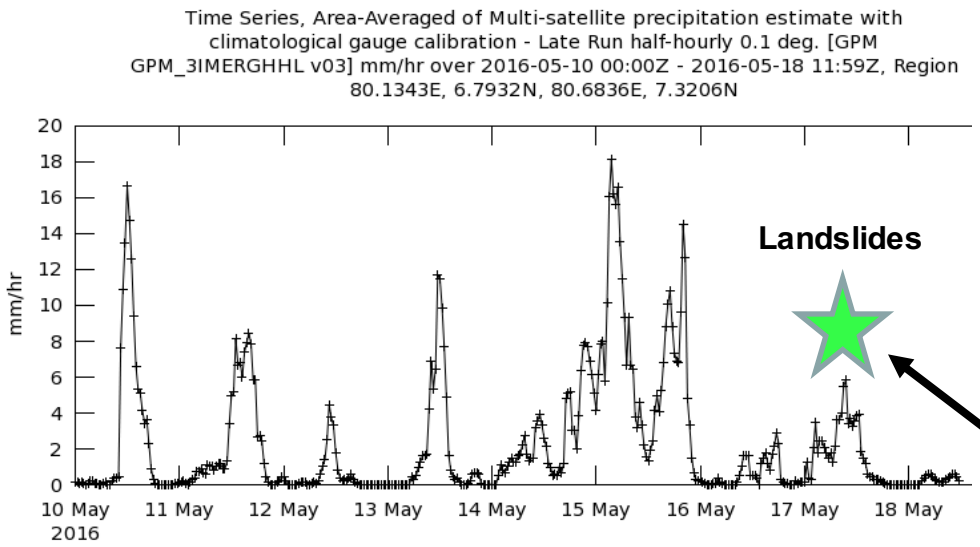


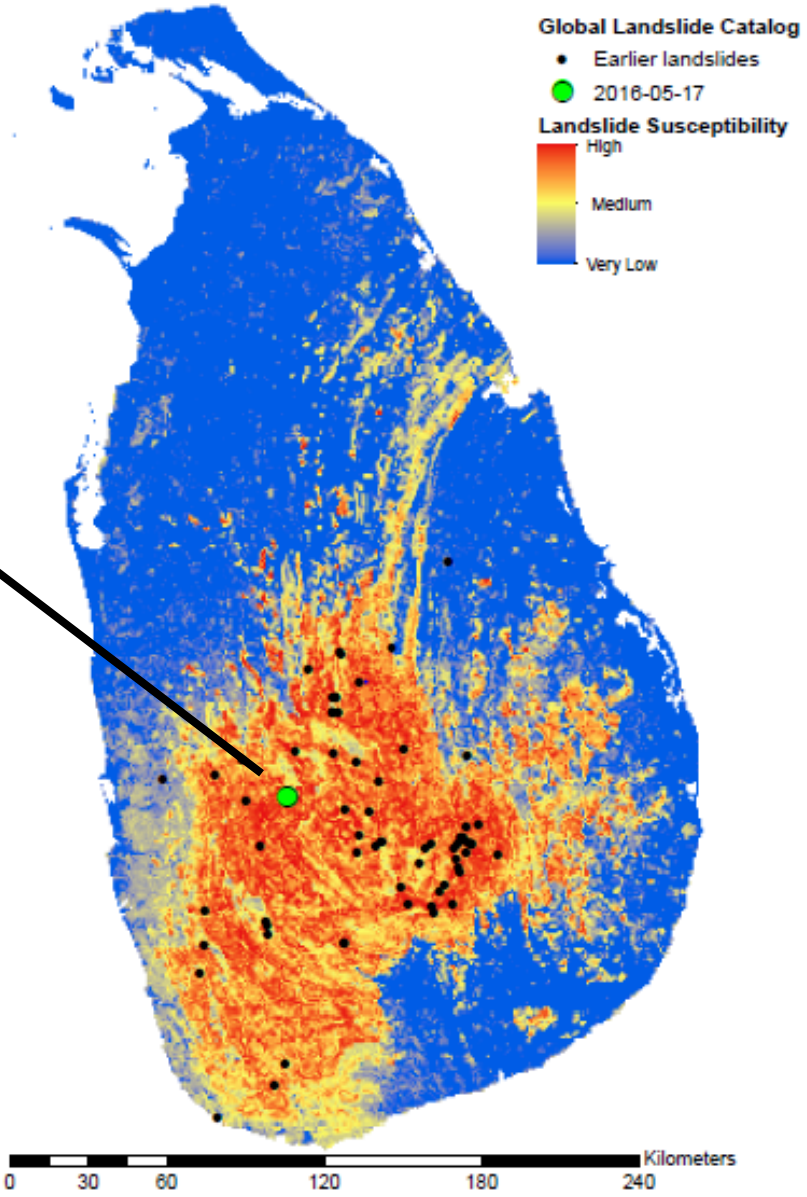


On the afternoon of May 17th, 2016, a major landslide event caused at least 92 deaths, with 109 still missing*. The site was rated highly susceptible to landslides in a new global landslide susceptibility map. GPM precipitation data suggest that both antecedent and current rainfall as well as complex topography played a role in the slope failures.

*BBC News (http://www.bbc.com/news/world-asia-36355980)

Name: Dalia Kirschbaum, Hydrological Sciences, NASA GSFC
E-mail: dalia.b.kirschbaum@nasa.gov
Phone: 301-614-5810

**References:**


- Time series, IMERG data (pmm.nasa.gov). Visualization of time series: NASA GES DISC Giovanni. J. G. Acker and G. Leptoukh, "Online Analysis Enhances Use of NASA Earth Science Data", *Eos, Transactions American Geophysical Union*, Vol. 88, No. 2 (9 January 2007), pages 14 and 17.
- Map: Stanley, T., and Kirschbaum, D., A heuristic approach to global landslide susceptibility mapping., In preparation for submission to *Natural Hazards*.
- Global Landslide Catalog: Kirschbaum, D., T. Stanley, and Y. Zhou, 2015: Spatial and temporal analysis of a global landslide catalog. Geomorphology, 249, 4–15, doi:10.1016/j.geomorph.2015.03.016. http://linkinghub.elsevier.com/retrieve/pii/S0169555X15001579.
- Background: BBC (2016), Sri Lanka mudslides: Death toll reaches 92 with many still missing, *BBC News*. Available from: http://www.bbc.com/news/world-asia-36355980 (Accessed 23 May 2016)


**Data Sources:**

- Rainfall: Integrated Multi-satellite Retrievals for GPM (IMERG)
- Elevation: Shuttle Radar Topography Mission, Advanced Spaceborne Thermal Emission and Reflection Radiometer, the Ice, Cloud, and land Elevation Satellite, and the Radarsat Antarctic Mapping Project
- Forest Loss: Landsat
- Geological features: Geological Map of the World
- Roads: OpenStreetMap
- Historical landslides: NASA's Global Landslide Catalog

**Technical Description of Figures:**

***Figure 1:*** Rainfall rate time series from IMERG data with 0.1-degree spatial resolution and 0.5-hour temporal resolution. Green star indicates approximate time of landslides.

***Figure 2:*** Excerpt from a global map of landslide susceptibility with a 30-arcsecond spatial resolution. Blue indicates areas with very low susceptibility to landslides, typically flat ground. Red indicates the presence of highly susceptible terrain. This map rates landslide susceptibility globally and might not be optimal for any specific region such as Sri Lanka.

**Scientific significance, societal relevance, and relationships to future missions:**

The global landslide susceptibility map is one component of a prototype landslide nowcasting system developed at GSFC. This system uses rainfall estimates from GPM and other satellites to provide current situational awareness, which enables faster, more informed disaster responses. The susceptibility map may also be used as an aid to prioritizing future research projects such as the remote sensing of landslides by optical or radar instruments.

# Calculating Remote Sensing Reflectance Uncertainties Using an Instrument Model Propagated Through Atmospheric Correction via Monte Carlo Simulations

E. Karakoylu, Ocean Ecology, SAIC, and B. Franz, Ocean Ecology, NASA GSFC, Carlos Del Castillo, Ocean Ecology, NASA GSFC

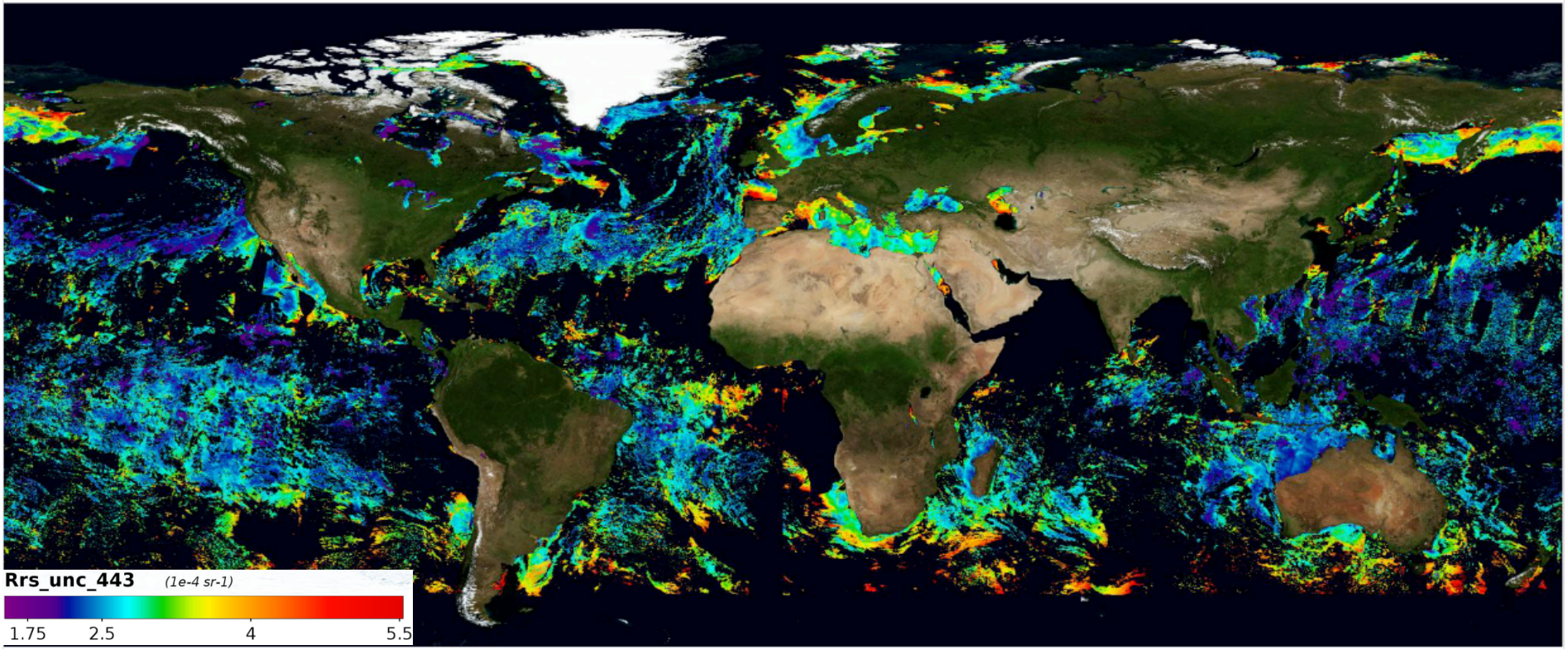


First attempt at quantifying uncertainties in ocean remote sensing reflectance satellite measurements. Based on 1000 iterations of Monte Carlo. Data source is a SeaWiFS 4-day composite, 2003. The uncertainty is for remote sensing reflectance (Rs) at 443 nm.

Name: Carlos E. Del Castillo, Ocean Ecology, NASA GSFC
E-mail: Carlos.e.delcastillo@nasa.gov
Phone: 301-286-8787

**References:**

New work

**Data Sources:** Remote sensing reflectance from SeaWiFS circa 2003. The same analysis can be applied to other sensors if a good instrument model is available.

**Technical Description of Figure:**

***Figure 1:*** Global distribution of uncertainties Rrs at 443 nm. Date are from 4 day composite SeaWiFS collected in 2003.

**Scientific significance, societal relevance, and relationships to future missions:** This is the first attempt at a quantifying total uncertainties in global ocean color data sets. These uncertainties in Rrs will be propagated through the science algorithms to produce uncertainty estimates for ocean color products. The methods developed here can be applied to past, current, and future ocean color missions.

# Measurement of the Band-to-Band Registration of the SNPP VIIRS Imaging System from On-Orbit Data

James C. Tilton, Terrestrial Information Systems, NASA GSFC, Guoging Lin, Terrestrial Information Systems, NASA GSFC and SSAI, and Bin Tan, Terrestrial Information Systems, NASA GSFC and SSAI

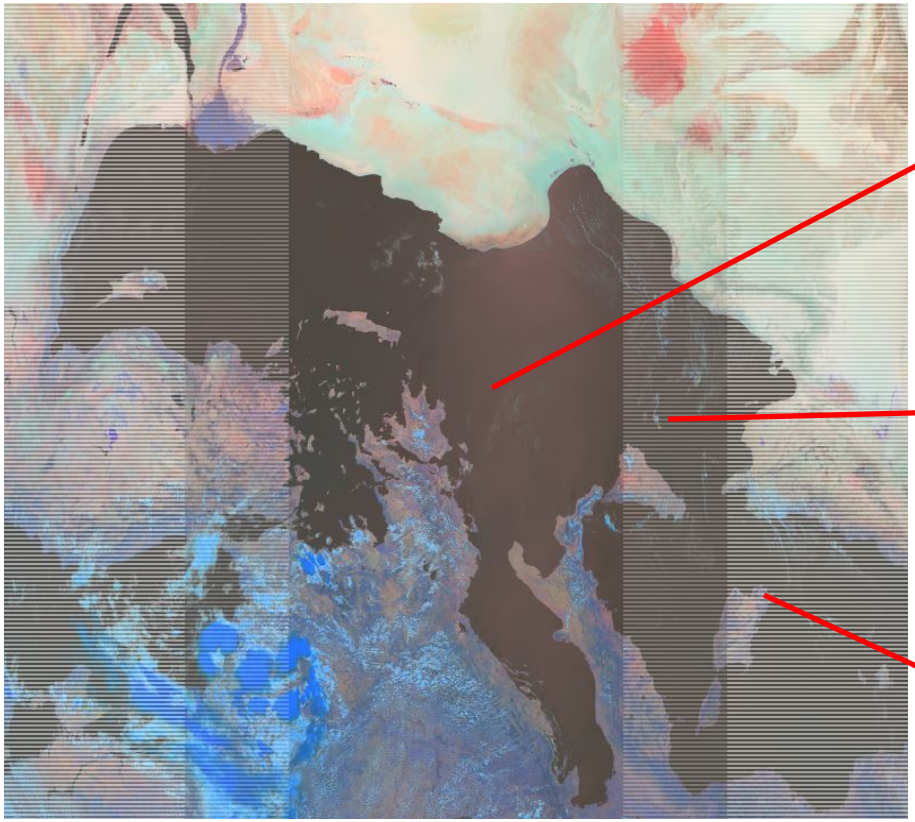

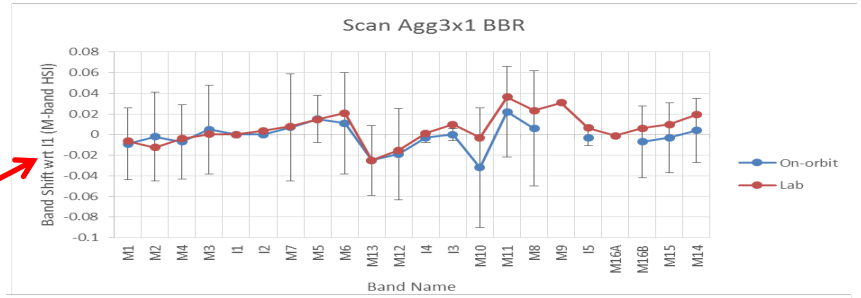


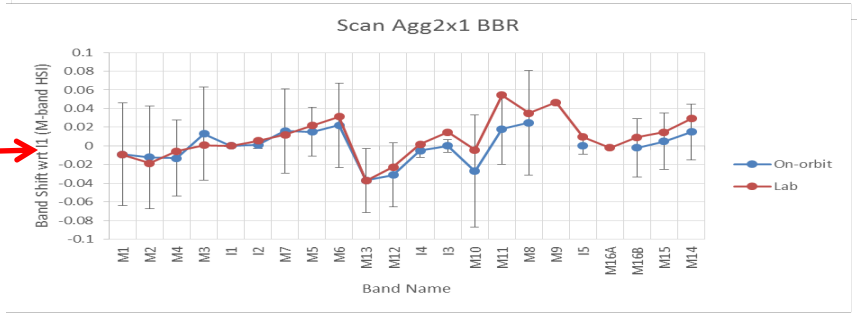


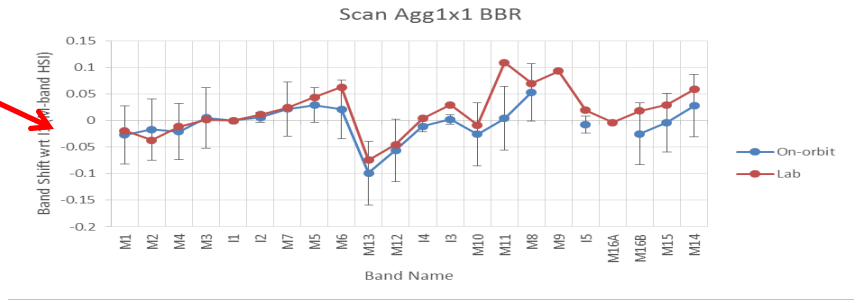


The on-orbit Band-to-Band measurements are generally in close agreement with pre-launch Band-to-Band measurements performed in a laboratory

Name: Bin Tan, Terrestrial Information Systems Lab, SSAI/NASA GSFC
E-mail: bin.tan@nasa.gov
Phone: 301-614-5965

**References:**

[1] C. Cao, F. J. De Luccia, X. Xiong, and F. Weng, "Early on-orbit performance of the visible infrared imaging radiometer suite onboard the Suomi National Polar-Orbiting Partnership (S-NPP) satellite," *IEEE Trans. Geosci. Remote Sens.*, vol. 52, no. 2, pp. 1142-1156, 2014.
[2] A. Gruen, "Development and Status of Image Matching in Photogrammetry," *The Photogrammetric Record*, vol. 27, pp. 36-57, 2012.
[3] A. A. Cole-Rhodes and P. K. Varshney, "Image registration using mutual information," in *Image Registration for Remote Sensing*, J. Le Moigne, N. S. Netanyahu and R. D. Eastman, eds, Cambridge: Cambridge University Press, pp. 131-149, 2011.
[4] Z. Wang, X Xiong and Y. Li, "Improved Band-to-Band Registration Characterization for VIIRS Reflective Solar Bands Based on Lunar Observations," *Remote Sensing*, vol. 8, no.27, pp. 1-12.
[5] G. Lin, J. C. Tilton, R. E. Wolfe, K. P. Tewari, and M. Nishihama, "SNPP VIIRS spectral bands co-registration and spatial response characterization," in *Proc. SPIE*, 2013, 8866, Art. ID. 88661G.
[6] J. P. Kern and M. S. Pattichis, "Robust multispectral image registration using mutual-information models," *IEEE Trans. Geosci. Remote Sens.*, vol. 45, no. 5, pp. 1494-1505, 2007.
[7] C. Studholme, D. L. G. Hill and D. Hawkes, "An overlap invariant entropy measure of 3D medical image alignment," *Pattern Recognition*, vol. 32, no. 1, pp. 71-86, 1999.
[8] K. I. Joy, "Catmull-Rom splines," *On-Line Geometric Modeling Notes*, (http://graphics.cs.ucdavis.edu/~joy/ecs278/notes/Catmull-Rom-Spline.pdf, last accessed Sep. 15, 2015).
[9] E. Catmull and R. Rom, "A class of local interpolating splines," in *Computer Aided Geometric Design*, R. E. Barnhill and R. F. Riesenfled, eds., New York: Academic Press, 1974.

**Data Sources:** VIIRS image from over the Mediterranean Sea collected on July 31, 2013.

**Technical Description of Figures:**

***Left Graphic:*** Imagery Resolution 5-Min L1 Swath Radiance data (bands I4, I3 and I2 shown as red, green and blue, respectively, with histogram equalization enhancement) for a VIIRS image from over the Mediterranean Sea collected on July 31, 2013. (Note: Since this image was acquired from an ascending orbit, the southeast corner is at the top-left corner as displayed.)

***Right Graphics:*** Plots of pre-launch (lab) and on-orbit measured BBR shifts for all bands versus band I1. One standard deviation error bars are included with the on-orbit measurements. (a) Along scan shifts in the 3x1 aggregation zone. (b) Along scan shifts in the 2x1 aggregation zone. (c) Along scan shifts in the no aggregation zone.

**Scientific significance, societal relevance, and relationships to future missions:** This is the first study to measure the band-to-band registration with on-orbit satellite data. The comparison to in-lab pre-launch BBR measurements shows that this set of algorithm, which include normalized mutual information and bicubic interpolation, produces accurate band-to-band registration assessment . The result also indicates that the VIIRS sensor is in good shape and performs as expected on band-to-band registration.